Astron. Astrophys. 315, L301–L304 (1996)

ASTRONOMY
AND
ASTROPHYSICS

Molecular hydrogen observations of Cepheus A West⋆

C.M. Wright[1], S. Drapatz[1], R. Timmermann[1], P.P. van der Werf[2], R. Katterloher[1], and Th. de Graauw[3]

[1] Max-Planck-Institut für extraterrestrische Physik, Postfach 1603, D-85740 Garching bei München, Germany
[2] Leiden Observatory, P.O. Box 9513, 2300 RA Leiden, The Netherlands
[3] Space Research Organisation of the Netherlands, P.O. Box 800, 9700 AV Groningen, The Netherlands

Received 17 July 1996 / Accepted 9 September 1996

Abstract. The Herbig–Haro complex GGD37 is an active region in the west of Cepheus A. We have used the ISO Short Wavelength Spectrometer (SWS) to investigate the physics of this region by observations of molecular hydrogen and forbidden atomic and ionic emission lines over a wide wavelength and excitation energy range. We find excitation temperatures of the emitting molecular gas to be between 700 and 11000 K, the former being thermal in nature, whilst the latter implies a contribution from non–thermal processes. Gas densities in the emitting region are at least 10^5 cm^{-3}. An H_2 ortho–to–para ratio of 3, equal to the ratio of statistical weights, is consistent with our observations. The forbidden transitions can be modelled by a planar J–shock with pre–shock density of 10^3 to 10^4 cm^{-3} and velocity 70 to 80 km s^{-1}. The H_2 lines cannot be fit by either a single planar J– or C–shock, but instead require a combination of at least two C–shocks with different pre–shock density, shock velocity and covering factor.

Key words: stars: pre-main sequence – ISM: individual objects: Cep A – ISM: jets and outflows – ISM: molecules – infrared: ISM: lines and bands

1. Introduction

The Herbig–Haro (HH) complex GGD37 is located at a distance of 730 pc in Cep A West, and forms part of the Cep A star forming region in the Cepheus OB3 molecular cloud complex. An illustration of the geometry of the region can be found in Corcoran, Ray and Mundt (1993, their Fig. 5), and a review of its properties has been presented by Staude and Elsässer (1993).

GGD37 is a region of strongly excited, shocked, atomic and molecular line emission. For example, Doyon and Nadeau (1988, hereafter DN88) mapped Cep A in the 2.122 μm 1–0 S(1) line of molecular hydrogen, finding several extended emission peaks, one of which, Peak 2, coincides with GGD37. Spectroscopy of the 1–0 S(1), 2.248 μm 2–1 S(1) and 2.424 μm 1–0 Q(3) lines of H_2 yielded line ratios and profiles consistent with shock excitation.

Hartigan et al. (1996, hereafter HEA96) obtained sub–arcsecond resolution images in the 1–0 S(1) line of H_2 and the [SII] lines at $\sim$ 6720 Å. They resolved the H_2 emission into many bow–shock like clumps and filaments, with fainter H_2 emission covering the entire area. From the spatial relationship between the H_2 and optical emission, HEA96 concluded that both continuous (C–) and jump (J–) shocks with magnetic precursor, of varying velocities (up to several hundred km s^{-1}, as derived from Hα line widths), are exciting the infrared and optical molecular and atomic/ionic emission in some of the different knots within GGD37.

2. Observations

We observed Cep A West in the SWS02 mode of the SWS (de Graauw et al. 1996) on board ISO (Kessler et al. 1996). The SWS Observer's Manual contains a detailed description of this mode. The SWS aperture was centred on Peak 2 of DN88, with RA = $22^h\ 54^m\ 06\overset{s}{.}5$ and δ = +61° 45′ 55″ (1950). Beam sizes were 14″ × 20″ for wavelengths up to 12 μm, 14″ × 27″ from 12 to 29.5 μm, and 20″ × 33″ from 29.5 to 45.2 μm. The long axis was oriented at a position angle (measured East of North) of 100°, which coincidentally is closely parallel to the long axis of the GGD37 nebula.

A list of the lines scanned for is given in Table 1. Reduction was carried out using standard Off Line Processing (OLP) routines up to the Standard Processed Data (SPD) stage within the SWS Interactive Analysis (IA) system. Between the SPD and Auto Analysis Result (AAR) stages, a combination of standard OLP and in–house routines were used to extract the individual spectra.

Send offprint requests to: C.M. Wright (MPE, Germany)

⋆ Based on observations with ISO, an ESA project with instruments funded by ESA Member States (especially the PI countries: France, Germany, The Netherlands and the United Kingdom) and with the participation of ISAS and NASA. The SWS is a joint project of SRON and MPE.

Table 1. ISO SWS observations and results for Cep A West

Line	Rest λ (μm)	Observing Time (s)	Observed Flux ($\times 10^{-20}$ W/cm^2)	Surface Brightness ($\times 10^{-12}$ W/cm^2/sr)
H_2 2–1 Q(1)	2.5510	600	0.895	1.36
H_2 1–0 Q(9)	2.5598	–	1.63	2.48
H_2 2–1 Q(5)	2.6040	400	$\leq$ 0.801	$\leq$ 1.22
H_2 1–0 O(2)	2.6269	400	3.12	4.75
H_2 1–0 Q(11)	2.6351	–	1.41	2.14
H_2 1–0 O(3)	2.8025	400	11.2	17.1
H_2 1–0 O(4)	3.0039	400	3.10	4.71
H_2 1–0 O(5)	3.235	600	6.53	9.93
H_2 0–0 S(9)	4.6946	400	12.2	18.5
H_2 0–0 S(7)	5.5112	200	25.4	38.6
H_2 0–0 S(5)	6.9095	400	53.2	80.9
H_2 0–0 S(4)	8.0251	600	24.5	37.3
H_2 0–0 S(3)	9.6649	200	38.6	58.7
H_2 0–0 S(2)	12.2786	1000	28.8	32.5
[Ne II]	12.8136	400	21.5	24.2
H_2 0–0 S(1)	17.0348	1200	15.7	17.7
[S I]	25.249	200	4.81	5.42
[Si II]	34.8141	400	83.5	53.8

3. Results

Spectra of the lines we observed toward Cep A West are presented in Fig. 1. All lines are unresolved and have Full Width at Half Maximum (FWHM) consistent with that expected from an extended source in the SWS aperture. i.e. within $\pm$ 30 km s^{-1} (ISO SWS Observer's Manual). Integrated line fluxes were computed from the product of the peak line intensity above noise and the observed FWHM. Since the images in HEA96 show that the emission region is extended well beyond our different apertures, we have converted our fluxes to surface brightnesses (intensities). For the H_2 lines this correction affects only the 0–0 S(1) and S(2) lines, which, compared to the other lines, are 25% fainter in surface brightness units than in flux units. The remaining line ratios are unaffected. Table 1 lists the observed fluxes and surface brightnesses.

The uncertainty in the observations is dominated by the present flux calibration uncertainty of about 30% of the SWS (Schaeidt et al. 1996). Statistical uncertainties, computed from the noise level near the line, are generally much smaller than this, as are uncertainties in uncorrected line ratios.

4. Discussion

4.1. Molecular hydrogen: extinction, temperature, ortho-to-para ratio and density

The excitation diagram in Fig. 2 shows a plot of the natural logarithm of the column density, corrected for the statistical weight, in the upper level of each transition detected versus the energy of that level, E_u. The excitation temperature, T_{ex}, of the gas is the reciprocal of the slope of the excitation diagram, and corresponds to the kinetic temperature in local thermodynamic equilibrium (LTE, e.g. Gredel 1994).

When calculating column densities in Fig. 2 we corrected our intensities for extinction using $A_{2.122\mu m}$=1.8$\pm$0.8 mag derived by DN88. We tried two extinction laws, those of Draine and Lee (1984) and Rieke and Lebofsky (1985), together with screen and mixed (McLeod et al. 1993) extinction models. All gave similar quantitative results. Error bars in Fig. 2 were calculated by propagating both the uncertainty in the flux calibration and the extinction.

In an excitation diagram using uncorrected intensities the 0–0 S(3) line at 9.6649 μm (i.e. in the middle of the silicate dust absorption feature) lies well below a line connecting the 0–0 S(4) and 0–0 S(2) lines at 8.0251 μm and 12.2786 μm respectively (i.e. in the wings of the silicate feature) implying significant differential extinction. Assuming that the S(2) and S(4) lines suffer no extinction we can derive a rough estimate of the extinction at 9.7 μm from the difference between the observed and expected column density of the S(3) line. This gives a $\tau_{9.7}$ of $\sim$0.9. Using $A_V/\tau_{9.7}$=18.5 from Roche and Aitken (1984), $A_V \sim 16$ mag toward GGD37. This agrees very well with the extinction estimate of DN88 when converted to A_V using standard interstellar extinction curves. As noted by DN88, such an apparently large extinction can be reconciled with the optical Herbig–Haro emission by postulating that the latter arises near the surface of the molecular cloud, whilst the H_2 emission occurs deeper in.

The statistical weight used in Fig. 2 includes a factor 3 for ortho–H_2 and 1 for para–H_2, due to the total nuclear spin of the molecule. It is evident that ortho– and para–H_2 lie on the same line in the excitation diagram, demonstrating that their abundance ratio is indeed 3, equal to the ratio of their statistical weights.

Figure 2 shows that a single excitation temperature is not appropriate for the molecular hydrogen in GGD37, but instead a range is inferred. Up to $E_u \approx$ 7000 K, T_{ex} is 700$\pm$30 K, referred to here as the "warm" H_2. This includes pure rotational transitions from S(1) through to S(5), as well as ro–vibrational transitions in the 1–0 O–branch. For E_u between 7000 and 12000 K the inferred T_{ex} is 2300$\pm$300 K, referred to here as the "hot" H_2, whilst from $E_u \approx$ 12000 to 16000 K T_{ex} is 11000$\pm$2000 K, referred to here as the "ultra–hot" H_2. Uncertainties indicate the temperature ranges obtained by varying $A_{2.122\mu m}$ between 1.0 and 2.6 mag, the extinction law, and the extinction model. Our T_{ex} for the hot H_2 is in good agreement with the 2400$\pm$300 K found by DN88.

The level populations of the warm and hot H_2 are likely determined by collisional excitation in the post–shock gas. In a study of a number of HH objects, Gredel (1994) found that a single excitation temperature of between 2000 and 2700 K could explain the H_2 level populations, and concluded that the upper levels, which were at energies between about 6000 K and 14000 K, were thermalised at these temperatures. We find a similar T_{ex} for our hot H_2 between the same energy range. However, ISO shows us that this temperature is not valid at lower and higher energies.

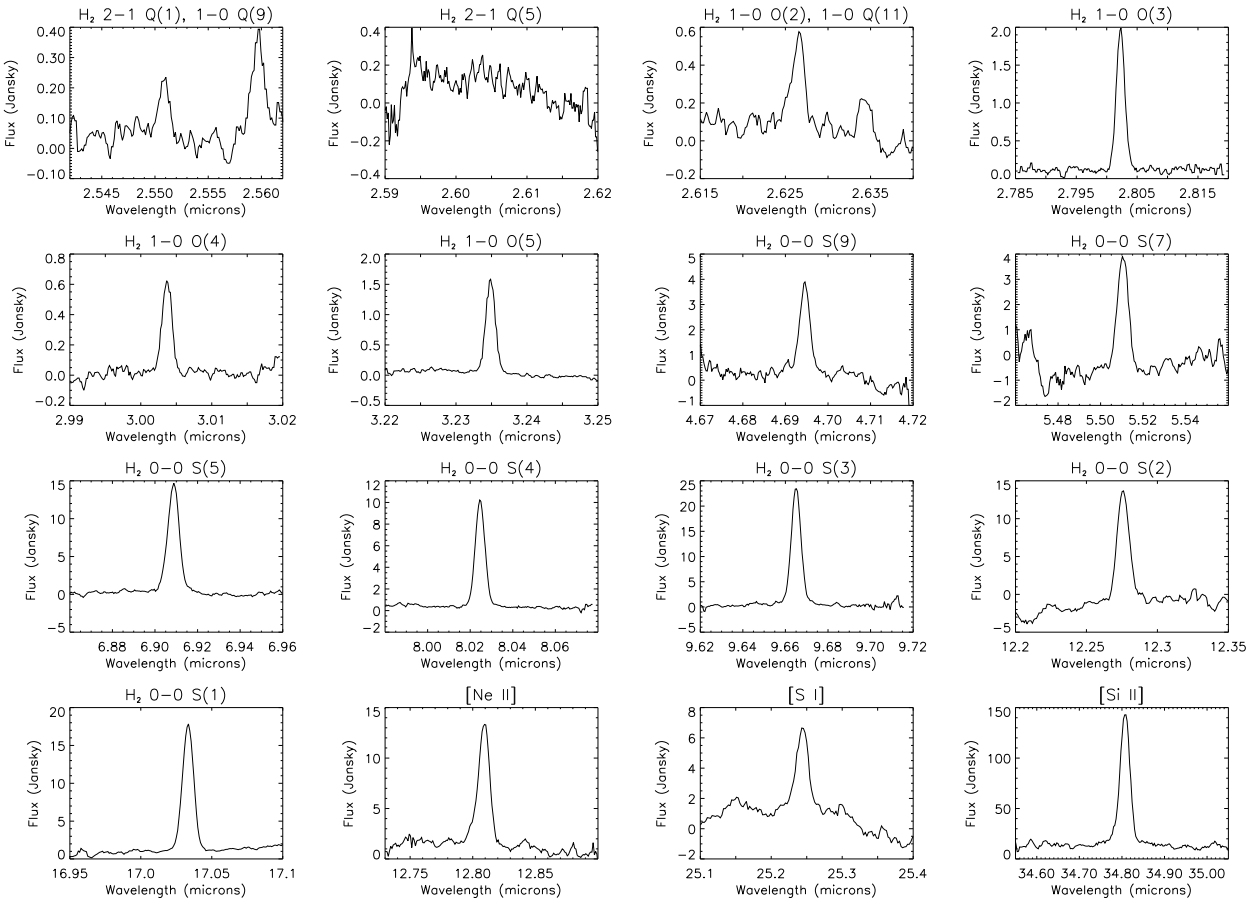

Fig. 1. ISO SWS spectra toward GGD37 in Cep A West. In two cases an additional line was detected, namely the H_2 1–0 Q(9) in the 2–1 Q(1) scan, and the H_2 1–0 Q(11) in the 1–0 O(2) scan. See Table 1 for their rest wavelengths

By calculating the critical density of the upper level of particular transitions we can derive a lower limit on the density of the post–shock gas, $n_{\rm post}$. Assuming that the upper level of the 0–0 S(5) line is thermalised at a temperature of 700 K then $n_{\rm post}$ ($=n_{\rm H_2}$) $\geq 10^5$ cm^{-3}, using the rate coefficients for H_2–H_2 collisions from Draine and Bertoldi (1996) and Einstein A–coefficients from Turner, Kirby–Docken and Dalgarno (1977). For H_2–H collisions (Mandy and Martin 1993), $n_{\rm post}$ ($=n_{\rm H}$) $\geq 5\times10^4$ cm^{-3}. For the upper level of the 1–0 O(2) line to be thermalised at 700 K, $n_{\rm post} \geq 10^8$ cm^{-3} for H_2–H_2 collisions, and $\geq 2\times10^5$ cm^{-3} for H_2–H collisions. If instead we consider the hot H_2, the upper levels of the 1–0 O(5), 0–0 S(9) and 2–1 Q(1) transitions are thermalised at 2000 K at $n_{\rm post} \geq 10^6$ cm^{-3} for H_2–H_2 collisions and $\geq 10^4$ cm^{-3} for H_2–H collisions. The aperture-averaged column density of the warm H_2 is $\sim 1.8\times10^{20}$ cm^{-2} and its mass is $\sim 10^{-2}$ M$_\odot$, whilst the corresponding values for the hot H_2 are $\sim 10^{18}$ cm^{-2} and $\sim 10^{-4}$ M$_\odot$.

Our detection of the ultra–hot H_2 is intriguing. A kinetic temperature of 10^4 K would result in substantial collisional dissociation of H_2 (Lepp and Shull 1983), so that the ultra–hot H_2 may more likely result from non–thermal processes populating the high energy levels. Plausible mechanisms include pumping by ultra–violet radiation and formation pumping of H_2 on dust grains in the cooling zone behind a dissociative shock. The non–detection of the H_2 2–1 Q(5) line may result from resonantly scattered Lyα photons that can selectively depopulate the upper level of this transition (Black and van Dishoeck 1987).

4.2. Comparison with published shock models

We consider first the atomic and ionic lines. We place most emphasis on the [Ne II] and [S I] lines, since [Ne II] is the most sensitive to shock velocity (Hollenbach and McKee 1989, hereafter HM89), and [Si II] is very dependent on uncertain dust destruction processes in shocks. The [Ne II]/[S I] ratio can be fit by a J–shock from HM89 with a pre–shock density (of H nuclei) of n_0=10^3 cm^{-3} and shock velocity $v_{\rm s}$=80 km s^{-1}, or n_0=10^4 cm^{-3} and $v_{\rm s}$=70 km s^{-1}. The [Si II]/[Ne II] ratio is also quite nicely fit by these two models. These respective models predict intensities factors of $\sim$ 10 and 2 below those observed, implying the shocks in GGD37 are viewed relatively edge–on (HM89).

However, the same shock parameters cannot fit the H_2 observations. This immediately suggests that the infrared atomic and ionic emission traces a different component of the cooling gas than the H_2 emission. The HM89 models produce thermal H_2

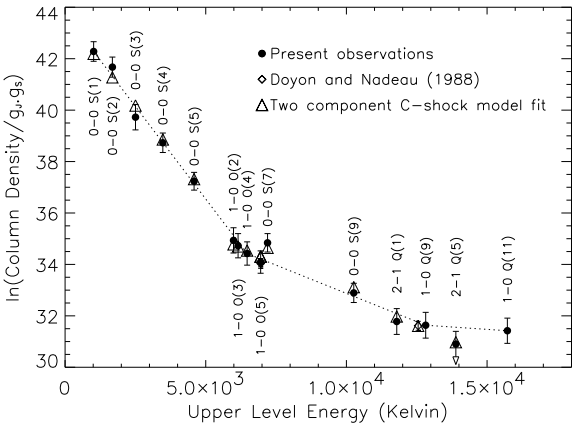

Fig. 2. H_2 excitation diagram for GGD37. The dashed lines indicate the different T_{ex} regions of the plot. The data have been corrected for an extinction of $A_{2.122\mu m}$=1.8±0.8 mag, a Draine and Lee (1984) extinction law, and a mixed extinction model. Two of the lines from DN88 share the same upper level as our 1–0 O(5) line

0–0 S(0) through S(5) emission from a region where molecules are re–forming in the cooling zone behind a dissociative shock, where the gas temperature is predicted to be 400–500 K. The ro–vibrational lines come from formation pumping. None of the shock models in HM89, for n_0=10^3–10^6 cm^{-3} and v_s=30–150 km s^{-1}, can fit our H_2 observations. The 0–0 S(1) through S(3) T_{ex} is always $\leq$ 450 K, significantly below our observed value of $\sim$ 700 K. Also, T_{ex} from the 1–0 S(1)/2–1 S(1) line ratio is always $\geq$ 4000 K, well above that found by DN88.

Burton, Hollenbach and Tielens (1992) extended the HM89 models to lower velocities, where the shock is non–dissociative. Our observed T_{ex} of the 0–0 S(3) through S(1) lines can be fit with n_0=10^4 cm^{-3} and v_s=10 km s^{-1}. An upper limit on T_{ex} from the model 1–0 S(1)/2–1 S(1) ratio is 4500 K. The predicted intensities are factors of $\sim$ 50 to 100 below the observed ones, again implying that the shocks in GGD37 are viewed close to edge–on. Unfortunately this exhausts the number of H_2 lines modelled by these authors. However, these non–dissociative shocks are more akin to C–shocks, and we now turn to them as a possible means of matching our observations.

A recent C–shock model is that of Kaufman and Neufeld (1996). A pre–shock density of n_{H_2}=10^4 cm^{-3}, magnetic field of $\sqrt{2n_{H_2}}$ μG, ionization fraction $\leq 10^{-7}$ and a shock speed of v_s=20 km s^{-1} provides a good match to our observed 0–0 S(1) through S(5) ratios (and so T_{ex}) and inferred upper level column densities. This same model cannot however reproduce the hot H_2 component we observe. A pre–shock density of 10^5 to 10^6 cm^{-3} and a shock velocity of 30–40 km s^{-1} is instead required. In this case T_{ex} of the 0–0 S(1) through S(5) lines, and inferred column densities, are too high. Therefore, in order to fit all our H_2 data we require a combination of two or more C–shocks with different initial conditions and different covering factors, Φ, the ratio of the emitting surface area of a shocked shell to the projected area of the beam (see Kaufman and Neufeld 1996).

A possible two component model fit is shown in Fig. 2. One shock is as described above, with Φ=0.5. The second shock has n_{H_2}= $10^{6.5}$cm^{-3}, v_s=35 km s^{-1} and Φ=0.001. Such a low covering factor for this second shock may be difficult to reconcile with the H_2 1–0 S(1) image of HEA96, which essentially fills our beam. We can increase it to 0.01 if the second shock instead has n_{H_2}=10^5 cm^{-3} and v_s=40 km s^{-1}, but in this case the inferred column densities in the 0–0 S(7) and S(9) upper levels are too high. We do point out however that our two component model is in qualitative agreement with the H_2 morphology of GGD37, namely that the first shock, being of a low density and large Φ, correponds to the extended emission, whilst the second shock, being of a high density and low Φ, corresponds to the clumpy emission. Similar qualitative results are obtained for the C–shock models of Draine, Roberge and Dalgarno (1983).

Clearly, no single planar shock into a uniform medium can simultaneously fit all our ISO observations of GGD37. Instead, both J– and C–shocks, with different pre–shock densities, velocities and covering factors must be invoked. If the shocks are bow–type, perhaps our atomic and ionic emission originates from the fast, dissociating and ionizing head, whilst the H_2 emission arises from the slower, non–dissociating wings.

Acknowledgements. The research of PvdW has been made possible by a fellowship of the Royal Netherlands Academy of Arts and Sciences. SWS and the ISO Spectrometer Data Centre at MPE are supported by DARA under grants 50 QI 8610 8 and 50 QI 9402 3.

References

Black, J. H., van Dishoeck, E. F., 1987, ApJ 322, 412
Burton, M. G., Hollenbach, D. J., Tielens, A. G. G. M., 1992, ApJ 399, 563
Corcoran, D., Ray, T. P., Mundt, R., 1993, A&A 279, 206
de Graauw, Th., et al., 1996, A&A, this issue
Doyon, R., Nadeau, D., 1988, ApJ 334, 883 (DN88)
Draine, B., Lee, H. M., 1984, ApJ 285, 89
Draine, B. T., Roberge, W. G., Dalgarno, A., 1983, ApJ 264, 485
Draine, B. T., Bertoldi, F., 1996, in preparation
Gredel, R., 1994, A&A 292, 580
Hartigan, P., Carpenter, J. M., Dougados, C., Skrutskie, M. F., 1996, AJ 111(3), 1278 (HEA96)
Hollenbach, D., McKee, C. F., 1989, ApJ 342, 306 (HM89)
Kessler, M. F., et al., 1996, A&A, this issue
Kaufman, M. J., Neufeld, D. A., 1996, ApJ 456, 611
Lepp, S., Shull, J. M., 1983, ApJ 270, 578
Mandy, M. E., Martin, P. G., 1993, ApJS 86, 199
McLeod, K. K., Rieke, G. H., Rieke, M. J., Kelly, D. M., 1993, ApJ 412, 111
Rieke, G. H., Lebofsky, M. J., 1985, ApJ 288, 618
Roche, P. F., Aitken, D. K., 1984, MNRAS 208, 481
Schaeidt, S. G., Morris, P. W., Salama, A., et al., 1996, A&A, this issue
Staude, H. J., Elsässer, H., 1993, A&AR 5, 165
Turner, J., Kirby–Docken, K., Dalgarno, A., 1977, ApJS 35, 281